C-Terminal Modulatory Domain Controls Coupling of Voltage-Sensing to Pore Opening in $Ca_v1.3$ L-type Ca^{2+} Channels

Andreas Lieb,[*] Nadine Ortner, and Jörg Striessnig[*]

Pharmacology and Toxicology, Institute of Pharmacy, and Center for Molecular Biosciences, University of Innsbruck, Innsbruck, Austria

ABSTRACT   Activity of voltage-gated $Ca_v1.3$ L-type Ca^{2+} channels is required for proper hearing as well as sinoatrial node and brain function. This critically depends on their negative activation voltage range, which is further fine-tuned by alternative splicing. Shorter variants miss a C-terminal regulatory domain (CTM), which allows them to activate at even more negative potentials than C-terminally long-splice variants. It is at present unclear whether this is due to an increased voltage sensitivity of the $Ca_v1.3$ voltage-sensing domain, or an enhanced coupling of voltage-sensor conformational changes to the subsequent opening of the activation gate. We studied the voltage-dependence of voltage-sensor charge movement (Q_{ON}-V) and of current activation (I_{Ca}-V) of the long ($Ca_v1.3_L$) and a short $Ca_v1.3$ splice variant ($Ca_v1.3_{42A}$) expressed in tsA-201 cells using whole cell patch-clamp. Charge movement (Q_{ON}) of $Ca_v1.3_L$ displayed a much steeper voltage-dependence and a more negative half-maximal activation voltage than $Ca_v1.2$ and $Ca_v3.1$. However, a significantly higher fraction of the total charge had to move for activation of $Ca_v1.3$ half-maximal conductance ($Ca_v1.3$: 68%; $Ca_v1.2$: 52%; $Ca_v3.1$: 22%). This indicated a weaker coupling of $Ca_v1.3$ voltage-sensor charge movement to pore opening. However, the coupling efficiency was strengthened in the absence of the CTM in $Ca_v1.3_{42A}$, thereby shifting I_{Ca}-V by 7.2 mV to potentials that were more negative without changing Q_{ON}-V. We independently show that the presence of intracellular organic cations (such as n-methyl-D-glucamine) induces a pronounced negative shift of Q_{ON}-V and a more negative activation of I_{Ca}-V of all three channels. These findings illustrate that the voltage sensors of $Ca_v1.3$ channels respond more sensitively to depolarization than those of $Ca_v1.2$ or $Ca_v3.1$. Weak coupling of voltage sensing to pore opening is enhanced in the absence of the CTM, allowing short $Ca_v1.3_{42A}$ splice variants to activate at lower voltages without affecting Q_{ON}-V.

INTRODUCTION

Ca^{2+} influx through voltage-gated Ca^{2+} channels (VGCCs) in the plasma membrane of electrically excitable cells causes membrane depolarization and triggers intracellular Ca^{2+}-dependent signaling processes. $Ca_v1.3$ and $Ca_v1.2$, members of the so-called L-type Ca^{2+} channel family (LTCCs, Ca_v1), are widely expressed in many tissues, including muscle and neurons, sensory tissue, and endocrine cells (1–5). Work with genetically modified mice revealed different physiological roles for these two channel isoforms, even when expressed in the same cell (6–8). Differences in their voltage- and Ca^{2+}-dependent gating properties underlie this functional diversity (6–8). $Ca_v1.3$ channels activate faster and at more negative voltages than $Ca_v1.2$ (9–11) and therefore sustain Ca^{2+} inward currents also at threshold voltages. This allows them to control autonomous pacemaking in the sinoatrial node (2,6) and adrenal chromaffin cells (7) and support upstroke potentials in neurons (12). $Ca_v1.3$ channels are also expressed in the substantia nigra

pars compacta dopaminergic neurons (13) where they seem to contribute to dendritic Ca^{2+} signals linked to mitochondrial stress and the selective vulnerability of these neurons in Parkinson's disease (14). Selective $Ca_v1.3$ channel block is currently pursued as a therapeutic option for neuroprotection in Parkinson's disease. Although $Ca_v1.3$ channels activate at voltages that are more negative than all other Ca_v1 ($Ca_v1.1$, $Ca_v1.2$, and $Ca_v1.4$) and Ca_v2 high VGCCs (15), they cannot be classified as low VGCCs, such as T-type channels (16). Indirect comparisons of published data suggest that T-type channels activate and inactivate at voltages that are more negative than $Ca_v1.3$ (16), but a direct comparison of their gating properties, to our knowledge, does not exist.

Within the past few years, we have discovered that the activation voltage range (I_{Ca}-V) of $Ca_v1.3$ Ca^{2+} inward currents (I_{Ca}) can be shifted to potentials that are even more negative by alternative splicing within the C-terminus of its pore-forming α_1-subunit (17,18). Alternative splicing generates $Ca_v1.3$ α_1-subunits with shorter C-termini (e.g., $Ca_v1.3_{42A}$, $Ca_v1.3_{43S}$ (18–20)) thereby removing a C-terminal modulatory domain (CTM) from long isoforms ($Ca_v1.3_L$). This causes two apparently independent changes of channel gating:

1. It moderates Ca^{2+}-induced inactivation (CDI), an important autoinhibitory feedback mechanism of the channel. The molecular basis of this effect is well understood. As in other VGCCs, CDI is induced by Ca^{2+} binding to calmodulin (CaM) preassociated with the

Editor: David Yue.

proximal C-terminus of α_1-subunits (21). The CTM of $Ca_v1.3$ competitively interferes with CaM binding, and thereby reduces CDI (17,21).

2. The presence of the CTM in long $Ca_v1.3$ splice variants reduces open probability at negative voltages and shifts the half-maximal activation voltage ($V_{0.5}(I_{Ca})$) by ~10 mV to potentials that are more positive. This modulation has been reported by different laboratories, and occurs independently of CaM (11,18,19).

In contrast to modulation of CDI, it remains unclear how the CTM can affect voltage-dependent gating. Contemporary homology models of the pore-forming α_1-subunit propose four voltage-sensing domains (transmembrane segments S1–S4 of each of the four homologous repeats), which undergo conformational changes upon de- and repolarization of the channel. The intramembrane movement of the four positively charged S4 helices represents the main moving part (22,23). The cytoplasmic linkers between S4 and S5 segments are tightly packed into the pore-forming segments (in particular S6 helices), and thereby couple the voltage-sensor movements (recorded as nonlinear charge movements Q_{ON} and Q_{OFF}) to pore opening and closing (22). In the case of $Ca_v1.3$, the CTM must therefore interfere with this gating apparatus to induce the positive shift in I_{Ca}-V. Mechanistically, two possibilities exist: the CTM could affect the voltage sensitivity of the voltage-sensing mechanism itself such that higher voltages are required to move the charged S4 helix (inducing a shift in Q_{ON} voltage-dependence (Q_{ON}-V)). Alternatively, it could decrease the efficiency of coupling between voltage-sensor movements and subsequent pore opening, evident as a change in I_{Ca}-V but not Q_{ON}-V parameters (24).

To address these questions, we established experimental conditions that allowed us to directly determine differences in gating properties that account for the more-negative I_{Ca}-V of $Ca_v1.3$ in comparison to $Ca_v1.2$ and of short $Ca_v1.3$ splice variants in comparison to long ones. We also systematically compared the gating properties of $Ca_v1.3$ with low-voltage-activated $Ca_v3.1$ T-type channels.

We found that $Ca_v1.3$ Q_{ON} is significantly more voltage-sensitive than Q_{ON} of $Ca_v3.1$ and $Ca_v1.2$. The coupling of voltage sensing to pore opening is less efficient in $Ca_v1.3$ but its negative Q_{ON}-V still leads to I_{Ca}-V that is more negative than in $Ca_v1.2$. The CTM did not affect the voltage-dependence of Q_{ON} of $Ca_v1.3$, indicating an inhibitory action on the transmission of voltage-sensor movements to pore opening. Surprisingly, intramembrane charge movement of $Ca_v3.1$ occurred at voltages more positive than that of $Ca_v1.3$, but the sensitive coupling of the voltage-sensors to pore opening accounted for low voltage activation of its I_{Ca}-V. In the course of our work, we also discovered a strong effect of intracellular organic cations on the voltage-sensing machinery of all three VGCCs.

METHODS

Cell culture and transient transfection

HEK 293 (human embryonic kidney) cells were grown in Dulbecco's modified Eagle's medium supplemented with 2 mM L-glutamine (Cat. No. 25030-032; Gibco, Life Technologies, Carlsbad, CA), 10 units/mL penicillin (Cat. No. P-3032; Sigma Aldrich, St. Louis, MO), 10 μg/mL streptomycin (Cat. No. S-6501; Sigma), and with 10% v/v fetal calf serum (Cat. No. 10270-106; Gibco). Cells were grown under 5% CO_2 and 37°C until they reached 80% confluency. They were split with 0.05% trypsin for cell dissociation, and passage did not exceed 20. Transient transfection was achieved as described in Bock et al. (19), using equimolar cDNA ratios encoding $Ca_v1.3_L$, $Ca_v1.2$, or $Ca_v3.1$ (generously provided by Norbert Klugbauer) together with auxiliary subunits β_3 and $\alpha_2\delta_1$. Cells were visualized by cotransfection of 1 μg GFP. Twenty-four hours after transfection, cells were plated on 35-mm polystyrene dishes, pretreated with 10 μg/mL poly-L-lysine. At 48–72 h after cell transfection, whole cell patch-clamp experiments were performed.

Whole-cell patch-clamp recordings

GFP-positive HEK 293 cells were recorded using the whole-cell patch-clamp configuration. Borosilicate glass electrodes, having a final resistance of 2–5 MΩ, were pulled with a micropipette puller (Sutter Instruments, Novato, CA) that was fire-polished (MF-830 microforge; Narishige, Tokyo, Japan). Data were digitized (Digitizer 1322A; Axon Instruments, Novato, CA) and recorded in the whole-cell patch-clamp configuration (Axopatch 200B; Axon Instruments).

Intracellular recording solutions used

$NMDG_{int}$: NMDG (150 mM n-methyl-D-glucamine), 10 mM EGTA, 1 mM $MgCl_2$, 10 mM HEPES, and 4 mM ATP-Mg, adjusted to pH 7.3 with MS (Methanesulfonate);

Cs_{int}: 135 mM CsCl, 10 mM Cs-EGTA, 1 mM $MgCl_2$, 10 mM HEPES, and 4 mM ATP-Na$_2$, adjusted to pH 7.3 with CsOH;

$TRIS_{int}$: 164 mM Tris, 10 mM EGTA, 1 mM $MgCl_2$, 10 mM HEPES, and 4 mM ATP-Mg, adjusted to pH 7.3 with MS; and

TEA_{int}: 160 mM TEA (triethanolamine), 10 mM EGTA, 1 mM $MgCl_2$, 10 mM HEPES, and 4 mM ATP-Mg, adjusted to pH 7.3 with MS.

Extracellular solution used for Q_{ON} recordings

Choline-$Cl(Mg^{2+})_{ext}$: 150 mM choline-Cl, 16 mM $MgCl_2$, 10 mM HEPES, 0.5 mM $CdCl_2$, and 0.2 mM $LaCl_3$, adjusted to pH 7.3 with CsOH.

Extracellular solutions used for I_{Ca} recordings

Choline-Cl_{ext}: 150 mM choline-Cl, 15 mM $CaCl_2$, 1 mM $MgCl_2$, and 10 mM HEPES, adjusted to pH 7.3 with CsOH;

Cs_{ext}: 150 mM CsCl, 15 mM $CaCl_2$, 1 mM $MgCl_2$, and 10 mM HEPES, adjusted to pH 7.3 with CsOH; and

$NMDG_{ext}$: 146 mM NMDG, 15 mM $CaCl_2$, 1 mM $MgCl_2$, and 10 mM HEPES, adjusted to pH 7.3 with HCl.

Cells were maintained at a holding potential of -80 mV, before a 25-ms-(I_{Ca}-V), or a 10-ms-long (Q_{ON}-V) square-pulse depolarization (2-s interpulse interval). P/4 leak subtraction was applied. Q_{ON} recordings were performed as described in Baig et al. (3).

To compare the Q_{ON}-V of $Ca_v1.3_L$ and $Ca_v1.3_{42A}$, we quantified Q_{ON} ($Q_{ON,\ max}$) at V_{rev} after applying conditional prepulses in 5-mV steps to different potentials as previously described in McDonough et al. (24) and Baig et al. (3). During depolarizations to V_{rev}, we measured the Q_{ON} not

already moved during the prepulse. This allowed calculation of Q_{ON}-V from the remaining Q_{ON} at V_{rev} after the indicated prepulses ($Q_{ON, post-pre}$). Using this protocol, we have previously also demonstrated that for Ca$_v$1.3$_L$, Q_{ON}-V is the same when Ca^{2+} in the extracellular solution is replaced by equimolar Mg^{+2} (+ 0.5 mM Cd^{2+} + 0.2 mM La^{3+}, see solutions above). This revealed no differences in surface charge effects and ruled out that the voltage-dependence of Q_{ON} is affected by the Mg^{2+}-based extracellular solution used to block ionic current for Q_{ON}-measurements (3).

Steady-state activation (G-V) relationships were derived from I_{Ca}-V curves. We did not analyze tail current-voltage relationships due to contamination of tail currents by off-gating current in Ca$_v$1.2 and Ca$_v$1.3 channels. I_{Ca}-V of individual experiments was fitted to a modified Boltzmann equation,

$$I = G_{max}(V - V_{rev})/\{1 + \exp[(-(V - V_{0.5}))/k_{act}]\},$$

where V_{rev} is the extrapolated reversal potential, V is the test potential, I is the peak current amplitude, G_{max} is the maximum slope conductance, $V_{0.5}$ is the half-maximal activation voltage, and k_{act} is the slope factor. For fitting I_{Ca}-V curves recorded in the presence of intracellular organic cations (no current reversal observed due to the lack of outward current), data points at test pulses to voltages >30–40 mV were excluded from fitting. Q_{ON}-V and steady-state activation curves (G-V) were fitted to a Boltzmann equation,

$$G(V) = G_{max}/\{1 + \exp[(-(V - V_{0.5}))/k_{act}]\},$$

where G_{max} is the saturating value and k_{act} is the slope factor. Junction potentials were individually calculated for every solution combination, using the software included in the PCLAMP 10.2 software suite (Molecular Devices, Sunnyvale, CA), and offline-subtracted. (Missing ion mobility values in PCLAMP 10.2 were collected from http://web.med.unsw.edu.au/phbsoft/mobility_listings.htm (accessed November 27, 2013)).

Junction potential corrections

Cs$_{int}$ versus choline-Cl$_{ext}$ (−9.3 mV);
NMDG$_{int}$ versus choline-Cl$_{ext}$ (−8.5 mV);
TEA$_{int}$ versus choline-Cl$_{ext}$ (−4 mV);
Tris$_{int}$ versus choline-Cl$_{ext}$ (−5.6 mV);
Cs$_{int}$ versus Cs$_{ext}$ (−2.4 mV);
Cs$_{int}$ versus NMDG$_{ext}$ (−13 mV);
NMDG$_{int}$ versus Cs$_{ext}$ (1.1 mV),
NMDG$_{int}$ versus choline-Cl(Mg^{2+})$_{ext}$ (−8.8 mV); and
Cs$_{int}$ versus choline-Cl(Mg^{2+})$_{ext}$ (−9.5 mV).

Statistics

Data were analyzed with the softwares CLAMPFIT 10.2 (Axon Instruments) and SIGMA PLOT 12 (Systat Software, Chicago, IL). For statistical analysis GRAPHPAD PRISM 5.1 software (GraphPad Software, La Jolla, CA) was used, performing either one-way ANOVA with Bonferroni post-hoc test or Student's t-test as given. Data are presented as mean ± SE. Significance level was set to α-error lower than $p < 0.05$ (*), $p < 0.01$ (**), and $p < 0.001$ (***).

RESULTS

Ca$_v$1.3 voltage sensors are highly sensitive to membrane potential changes but are weakly coupled to activation of ion conductance

To compare the voltage-dependence of charge movement (Q_{ON}-V) with the I_{Ca}-V of different VGCCs we had to establish experimental conditions for reproducible recordings of Q_{ON} over a large voltage range. This was achieved by using rat Ca$_v$1.3 α_1-subunits that express at higher levels than human channels (but with indistinguishable current properties (25)) and by replacing Cs$^+$ in our intracellular standard solution with NMDG to prevent contaminating outward currents. Inward currents were blocked by replacing Ca^{2+} with isomolar concentrations of Mg^{2+} and addition of 0.5 mM CdCl$_2$ and 0.2 mM LaCl$_3$. Using a prepulse protocol (Methods; see also below), we have previously shown that the voltage-dependence of Q_{ON} is not affected by this solution exchange (3) and direct comparisons of I_{Ca}-V and Q_{ON}-V are possible without corrections for surface charge shifts, as discussed in previous studies (24,26). Representative recordings of I_{Ca} (left panel) and Q_{ON} (right panel) for Ca$_v$1.3$_L$, Ca$_v$1.2, and Ca$_v$3.1 at different test potentials are illustrated in Fig. 1.

As in previous studies with Cs$^+$-solution (3,18,25), the long splice variant of Ca$_v$1.3 (Ca$_v$1.3$_L$) became activated at a voltage range that is more negative than Ca$_v$1.2 under identical experimental conditions with NMDG as the major intracellular cation (Fig. 2 A). Ca$_v$1.3$_L$ activated with a half-maximal activation voltage ($V_{0.5}(I_{Ca})$) of ~10 mV more negative than Ca$_v$1.2 (Fig. 2 A; for statistics, see Table 1). To test whether this was due to a more refined voltage sensing, we also measured Q_{ON}-V. Although the threshold voltage for induction of Q_{ON} was similar for both channels, Ca$_v$1.3$_L$ displayed a steeper voltage-dependence as evident from the significantly lower slope factor and more-negative half-maximal activation voltage of Q_{ON} ($V_{0.5}(Q_{ON})$) (Fig. 2 B; and see Table 1 for statistics). A comparison of conductance (G-V) and Q_{ON}−V is shown in Fig. 1 C.
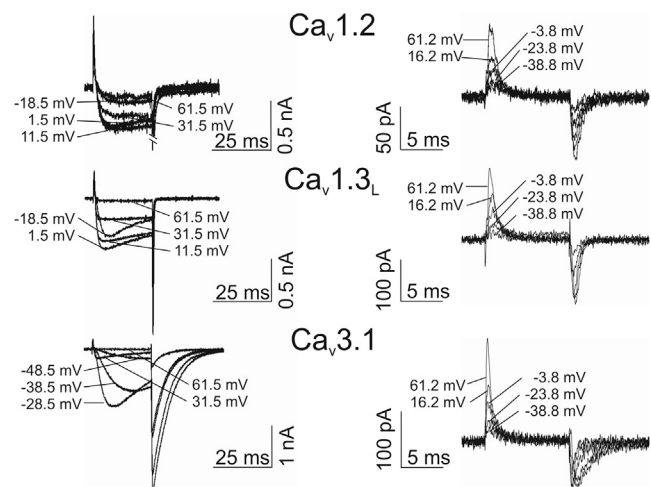

FIGURE 1 Representative current traces of I_{Ca} and Q_{ON}. Representative current traces of I_{Ca} (left) and Q_{ON} (right) are shown for Ca$_v$1.2, Ca$_v$1.3$_L$, and Ca$_v$3.1 at different depolarizing voltages.
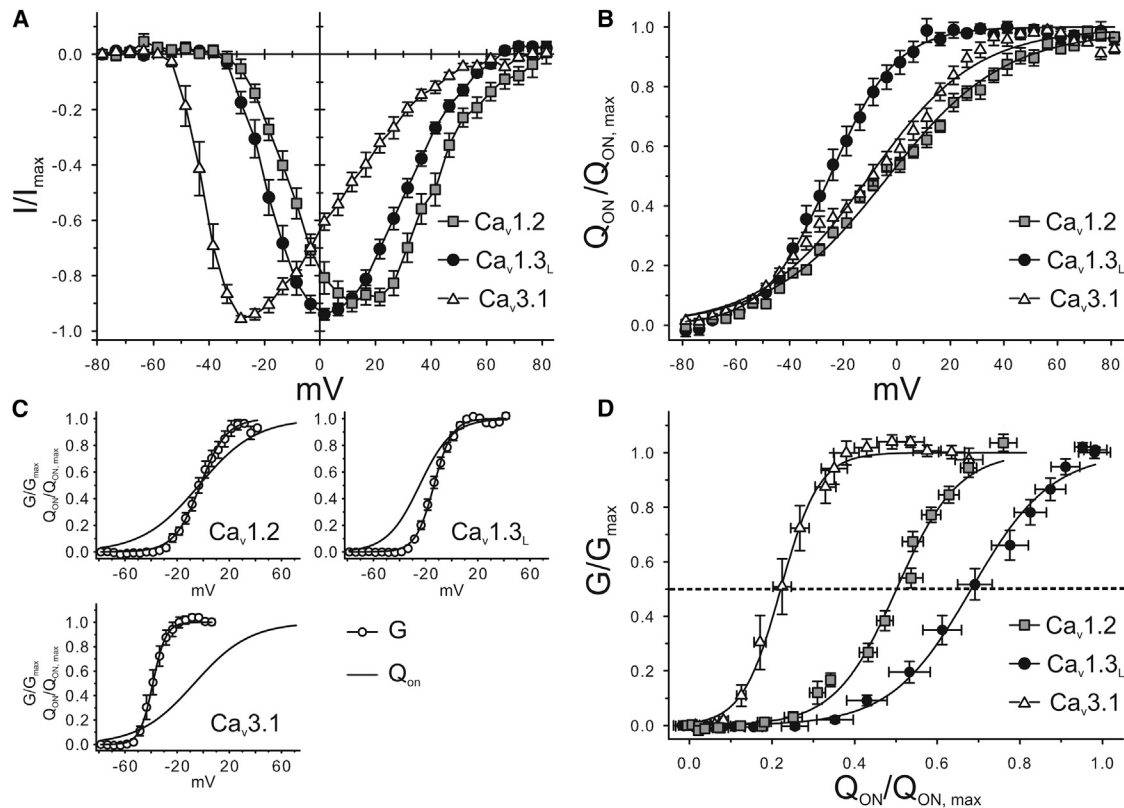
FIGURE 2 I_{Ca} and Q_{ON} voltage-dependence of $Ca_v1.2$, $Ca_v1.3_L$, and $Ca_v3.1$. The n-numbers and detailed statistics are given in Table 1. (*A*) Normalized I_{Ca}-V recorded with standard extracellular solution (choline-Cl_{ext}) and intracellular NMDG ($NMDG_{int}$). I_{Ca}-V was fitted to a modified Boltzmann function, as described in Methods. (*B*) Normalized Q_{ON}-V of $Ca_v1.2$, $Ca_v1.3_L$, and $Ca_v3.1$ recorded with choline-$Cl(Mg^{2+})_{ext}/NMDG_{int}$. (*C*) Comparison of the voltage-dependence of Q_{ON} (*solid line*, Boltzmann fit from data in panel *B*) and conductance (*G*, calculated from data shown in panel *A*). (*D*) Normalized G/G_{max} in comparison to normalized $Q_{ON}/Q_{ON, max}$ measured at similar voltages (difference = 0.3 mV) to illustrate the fraction of observed gating charge required for activation of conductance. (*Dashed line*) Half-maximal conductance. Data points were obtained from the experiments given in Table 1. Pooled data were fitted to a sigmoid function to determine the fractional Q_{ON} at half-maximal G. Values were significantly different among the three channels (determined by sum-of-squares F-test from GRAPHPAD PRISM, GraphPad Software).

As a measure for the efficiency of voltage-sensor charge movement to pore opening, we plotted the fraction of total observed Q_{ON} ($Q_{ON}/Q_{ON, max}$), required for the activation of G (G/G_{max}) at each voltage (Fig. 2 *D*). Fitting the data to a sigmoid function revealed that significantly less total Q_{ON} (52%, $n = 10$) was required to activate half-maximal conductance of $Ca_v1.2$ than of $Ca_v1.3_L$ (68%, $n \geq 13$) (see legend to Fig. 2 *D*). These data indicate weaker coupling of voltage-sensor movements to pore opening in $Ca_v1.3$ as compared to $Ca_v1.2$. However, the more-sensitive Q_{ON} charge movement still results in activation at voltages that are more negative than $Ca_v1.2$. Low-VGCCs (T-type; Ca_v3 family (27)) are known to activate at significantly lower voltages than $Ca_v1.3_L$ (28,29), also shown in our direct comparison with $Ca_v1.3_L$ (Fig. 2 *A*). This can be explained by the finding that only a small fraction of total $Ca_v3.1$ Q_{ON} (22%, $n \geq 9$; Fig. 2, *B–D*; and see Table 1) was required for half-maximal activation of conductance. This allows $Ca_v3.1$ I_{Ca} to activate at much lower voltages than Cav1.3 despite its more positive Q_{ON}-V, which is similar to $Ca_v1.2$ (Fig. 2 *B*).

Our data show that the voltage-sensing machinery of $Ca_v1.3$ responds more sensitively to depolarizing stimuli than $Ca_v1.2$ and even $Ca_v3.1$. Despite its weaker coupling to pore opening, this allows $Ca_v1.3_L$ to carry I_{Ca} at voltages that are more negative than for $Ca_v1.2$.

Alternative splicing affects Q_{ON} coupling to pore opening of $Ca_v1.3$ LTCCs

We next investigated whether the more-negative I_{Ca}-V previously observed for naturally occurring C-terminally short splice variants (such as $Ca_v1.3_{42A}$) as compared to the long $Ca_v1.3_L$ splice variants (18,19) is attributable to more refined voltage sensing or more efficient pore coupling. A negative shift was also observed when intracellular NMDG was used instead of Cs^+ (Fig. 3, *A* and *C*) as in previous studies (18,19). The $V_{0.5}(I_{Ca})$ for $Ca_v1.3_{42A}$ was 7 ± 2 mV more negative (Fig. 3 *A*; for statistics, see Table 1) and inactivation of I_{Ca} was faster (due to more pronounced CDI as demonstrated in previous work (18)). Measuring Q_{ON} for this short splice variant was more

TABLE 1 Biophysical properties of VGCCs α_1-subunits

choline-Cl$_{ext}$ / NMDG$_{int}$	V$_{0.5}$(I$_{Ca}$) [mV]	Slope (I$_{Ca}$) [mV]	n
Ca$_v$1.2	−3 ± 2	8.6 ± 0.6	10
Ca$_v$1.3$_L$	−13 ± 1 ***	6.4 ± 0.3 **	14
Ca$_v$1.3$_{42A}$	−20 ± 2 ***, †	5.6 ± 0.3 ***	17
Ca$_v$3.1	−40 ± 2 ***, †††, ‡‡‡	3.8 ± 0.3 ***, †††, ‡‡	12
choline-Cl$_{ext}$ / Cs$_{int}$			
Ca$_v$1.2	14 ± 2 §§§	11.2 ± 0.5 §§	28
Ca$_v$1.3$_L$	−4 ± 1 §§§	8.8 ± 0.2 §§§	19
Ca$_v$3.1	−35 ± 1 §	5.3 ± 0.2 §§§	11
choline-Cl(Mg^{2+})$_{ext}$ / NMDG$_{int}$	**V$_{0.5}$(Q$_{ON}$) [mV]**	**Slope (Q$_{ON}$) [mV]**	**n**
Ca$_v$1.2	−3 ± 2	22.6 ± 1.3	10
Ca$_v$1.3$_L$	−24 ± 2 ***	11.6 ± 0.9 ***	13
Ca$_v$3.1	−6 ± 2 †††	19.9 ± 0.9 †††	10
choline-Cl(Mg^{2+})$_{ext}$ / NMDG$_{int}$	**V$_{0.5}$(Q$_{ON}$) at V$_{rev}$ [mV]**	**Slope (Q$_{ON}$) at V$_{rev}$ [mV]**	
Ca$_v$1.3$_L$	−29 ± 3	10.6 ± 1.9	12
Ca$_v$1.3$_{42A}$	−27 ± 2	11.1 ± 0.7	10

Parameters (mean ± SE) were obtained by fitting data of I$_{Ca}$-V relationships or by fitting data of Q$_{ON}$-V relationship, as described in methods. Q$_{ON}$-V was either determined by measuring Q$_{ON}$ during pulses to different voltage steps or by measuring Q$_{ON}$ at V$_{rev}$ after prepulses to different voltages (V$_{0.5}$(Q$_{ON}$) at V$_{rev}$). Statistical significances are indicated for comparison vs. Ca$_v$1.2 (*, **, ***), vs. Ca$_v$1.3$_L$ (†, ††, †††), and vs. Ca$_v$1.3$_{42A}$ (‡, ‡‡, ‡‡‡) (one-way ANOVA with Bonferroni post-hoc test). §, §§, §§§ indicate statistical significance for intra-construct comparisons of parameters obtained with intracellular NMDG vs intracellular Cs (e.g. Ca$_v$1.2 choline-Cl$_{ext}$/NMDG$_{int}$ vs. Ca$_v$1.2 choline-Cl$_{ext}$/Cs$_{int}$) (Student's t-test).

difficult than for Ca$_v$1.3$_L$ due to small (presumably Mg^{2+}) inward currents contaminating the measurement of Q$_{ON}$ at voltages at ~V$_{max}$, but not at V$_{rev}$. We therefore determined Q$_{ON}$-V at V$_{rev}$ (Fig. 3 B) by measuring Q$_{ON}$ that remained after applying conditioning prepulses to different voltages (see Methods).

Such prepulses moved part of Q$_{ON}$ in a voltage-dependent manner and allowed calculation of Q$_{ON}$-V from the remaining Q$_{ON}$ at V$_{rev}$ after the indicated prepulses (Q$_{ON, post-pre}$). This protocol has originally been described by McDonough et al. (24) and was validated by us previously (3) and in this study (see legend to Fig. 3 B). Despite the more-negative V$_{0.5}$(I$_{Ca}$) for Ca$_v$1.3$_{42A}$, no significant difference in the Q$_{ON}$-V was observed between long and short Ca$_v$1.3 constructs (Fig. 3 B; for statistics, see Table 1). G-V curves for both splice variants are shown in Fig. 3 C in relation to their Q$_{ON}$-V (for analysis, see Fig. 2 D). Half-maximal G of Ca$_v$1.3$_{42A}$ required significantly less Q$_{ON}$ than the long isoform (68 vs. 79%, n ≥ 10) (Fig. 3 D). Taken together, these findings demonstrate that the presence of the intramolecular protein interaction forming the CTM in Ca$_v$1.3 LTCCs modulates the I$_{Ca}$-V activation of Ca$_v$1.3 by reducing the coupling efficiency between voltage sensing and pore opening.

Cation composition strongly affects voltage-dependent VGCC gating

Comparison of our I$_{Ca}$-V relationships measured using intracellular NMDG (Figs. 2 and 3) with our previously published data employing intracellular Cs$^+$ revealed an ~10 mV shift of V$_{0.5}$(I$_{Ca}$) toward voltages that were more negative for Ca$_v$1.3$_L$ (Fig. 4 A). In these experiments, an identical extracellular solution with choline as the major extracellular cation, and 15 mM Ca^{2+} as the charge carrier, was employed (3,9,18,19,25) (Fig. 4 A). We corrected all data for junction potentials precisely calculated for all our solutions as described in the Methods, ruling out differences in junction potentials as an explanation for this difference. To further characterize this unexpected finding, we also recorded Ca$_v$1.2 and Ca$_v$3.1 I$_{Ca}$-V relationships with NMDG (NMDG$_{int}$) or Cs$^+$ containing intracellular solution (Cs$_{int}$). This revealed a negative shift also for these channel types (Table 1) and thus ruled out a Ca$_v$1.3-specific effect of NMDG. Next, we tested whether the effect was mimicked by other large organic cations. Tris and TEA caused a similar negative shift of I$_{Ca}$-V like NMDG as shown for Ca$_v$1.3$_L$ (Fig. 4 D). We also quantified effects on Q$_{ON}$ for Ca$_v$1.3$_L$. Intracellular NMDG also shifted Q$_{ON}$-V by approximately the same extent as I$_{Ca}$-V (Fig. 4 B, inset; Ca$_v$1.3$_L$: n = 12; Ca$_v$1.3$_{42A}$: n = 9; p = 0.02, Student's t-test), suggesting that the NMDG effect is due to voltage-sensing that is more refined rather than by pore-coupling (Fig. 4 C).

To test whether changes in the voltage-dependence of gating are also observed by corresponding changes of the extracellular solution, we exchanged choline-Cl (in our standard extracellular solution) by either CsCl (Cs$_{ext}$) or NMDG-Cl (NMDG$_{ext}$), closely resembling the changes in the internal solutions. The V$_{0.5}$(I$_{Ca}$) values obtained with the various combinations of intra- and extracellular solutions are illustrated in Fig. 4 D. When intracellular Cs$^+$ was present, the replacement of extracellular choline by NMDG or Cs$^+$ did not cause a change in V$_{0.5}$(I$_{Ca}$). Intracellular NMDG also caused a negative shift with extracellular Cs$^+$, as observed with extracellular choline. Taken together, our data revealed that intracellular but not extracellular organic cations can enhance the coupling efficiency of Ca^{2+} channel voltage sensors to membrane depolarization.

DISCUSSION

Our study was motivated by two previous observations regarding Ca$_v$1.3 function:

1. Ca$_v$1.3$_L$ channels were previously reported to activate at lower voltages than Ca$_v$1.2. This special feature has been discovered in heterologous expression studies (9,10) but was subsequently confirmed for native Ca$_v$1.3 currents in sinoatrial node cells (6), cochlear
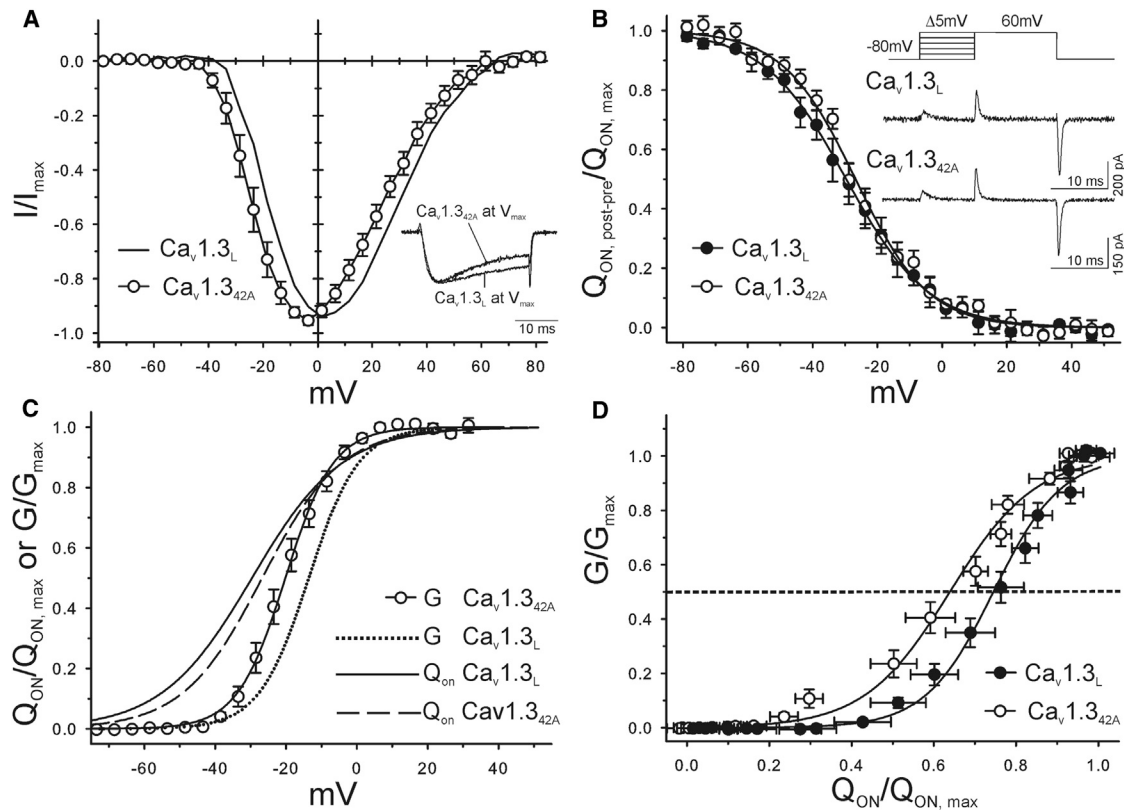
FIGURE 3 I_{Ca} and Q_{ON} voltage-dependence of $Ca_v1.3_L$ in comparison to $Ca_v1.3_{42A}$. The n-numbers and detailed statistics are given in Table 1. (A) I_{Ca}-V of $Ca_v1.3_L$ and $Ca_v1.3_{42A}$ recorded with standard recording solutions (choline-Cl_{ext}/$NMDG_{int}$). Fits were generated as described in Fig. 2 A. (B) Q_{ON}-V measured for $Ca_v1.3_L$ ($n = 12$) and $Ca_v1.3_{42A}$ ($n = 10$) using the prepulse protocol (inset) as described in Methods with Mg^{2+}-containing solution. (Inset) Example traces for both constructs obtained by depolarization to the reversal potential after a prepulse to −28.8 mV, which causes partial movement of Q_{ON}. The value Q_{ON} after the prepulse ($Q_{ON, post-pre}$) was normalized to $Q_{ON, max}$. For $Ca_v1.3_L$ the same gating parameters were obtained using this and the protocol in Fig. 2 B. (C) Comparison of the Q_{ON}-V and G-V relationships of $Ca_v1.3_L$ and $Ca_v1.3_{42A}$. (Solid and dashed lines) Boltzmann fits of Q_{ON}-V data obtained from experiments illustrated in panel B (dotted line is the same as in Fig. 2 C ($Ca_v1.3_L$) for comparison). (D) Data representation as in Fig. 2 D. Data points were obtained from the experiments given in Table 1. Pooled data were fitted to a sigmoid function to determine the fractional Q_{ON} at half-maximal G. Values were significantly different between the two splice variants (determined by sum-of-squares F-test using GRAPHPAD PRISM, GraphPad Software).

inner hair cells (2), and adrenal chromaffin cells (7). It allows $Ca_v1.3$ channels to sustain subthreshold inward currents and thus serve as a pacemaker channel in the sinoatrial node and chromaffin cells and shape firing patterns of neurons (12).

2. C-terminal splicing removes a CTM (11,18,19), which can further shift the channel's I_{Ca}-V to more-negative voltages in short splice variants.

Because these splice variants are expressed in a tissue-dependent manner, it is likely that they contribute to the fine-tuning of $Ca_v1.3$ channel activity in different tissues. Here we present data showing that the voltage sensors of $Ca_v1.3$ respond more readily to depolarizing stimuli than those of $Ca_v1.2$ and $Ca_v3.1$. This ensures that despite the weaker coupling of voltage sensing to pore opening, $Ca_v1.3$ currents can activate at lower membrane potentials than $Ca_v1.2$. Moreover, alternative splicing enhances the efficiency of coupling between charge movement and pore opening, explaining the even lower activation voltage

range of naturally occurring short splice variants lacking the CTM.

Based on contemporary structural models of the voltage-gated cation channel family, mainly derived from x-ray structures of voltage-gated K^+- (30) and bacterial Na^+-channels (31), a negative shift in the voltage-dependence of channel conductance (G-V) may, in principle, result via two possible mechanisms:

1. Values of Q_{ON}-V that are more negative. Even if the efficiency of voltage-sensor coupling to the pore remains unchanged, this should shift G-V to voltages that are more negative. An example is the deletion of a 'gating brake' in T-type channel α_1-subunits. This causes a negative shift and steeper voltage-dependence (slope) of the Q_{ON}-V relationship (29) paralleled by a corresponding negative shift in G-V (32).

2. Q_{ON}-V is unaltered but the efficiency of coupling to pore opening is enhanced. This has been reported for the LTCC activators FPL64176 and BayK8644, which induce strong
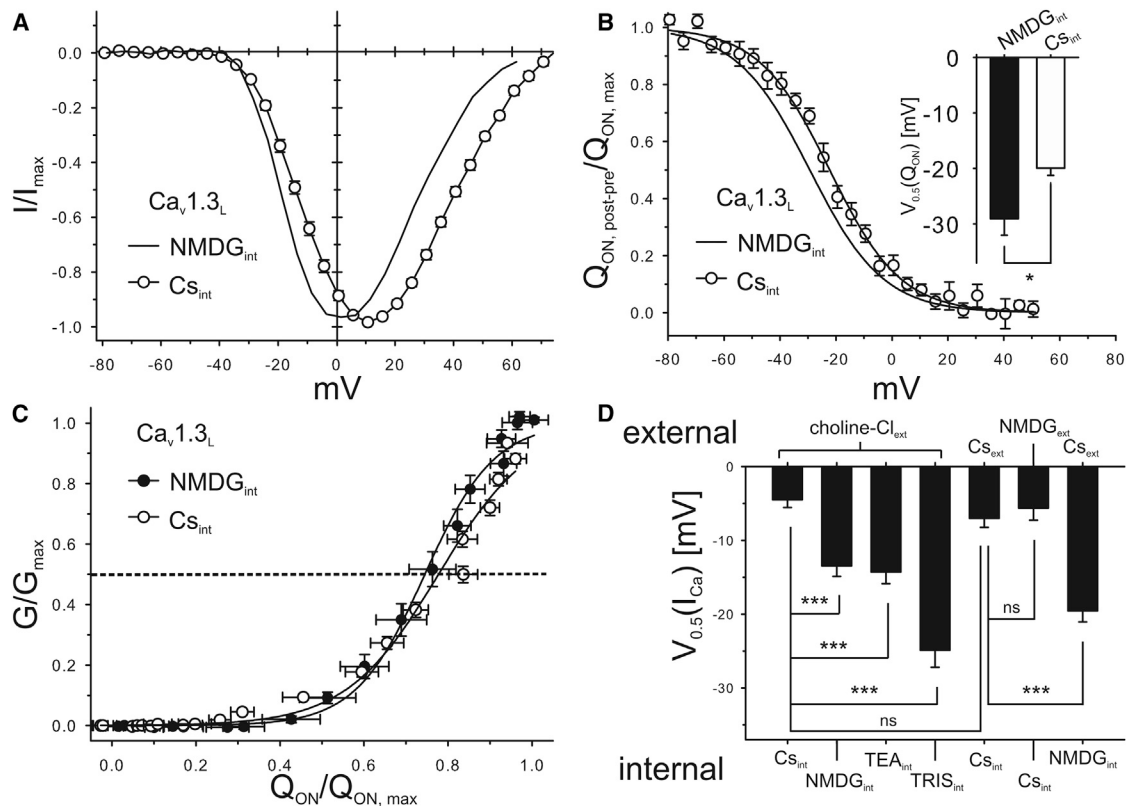
FIGURE 4 Effect of intracellular cations on Ca$_v$1.3$_L$ voltage-dependence. (A) I_{Ca}-V of Ca$_v$1.3$_L$ recorded with either Cs_{int} or $NMDG_{int}$. (For comparison, I_{Ca}-V of Ca$_v$1.3$_L$ recorded with $NMDG_{int}$ is shown as a *line*, as taken from Fig. 2 A.) Fits were generated as described in Fig. 2 A. For statistics, see panel D. (B) Q_{ON}-V of Ca$_v$1.3$_L$, recorded at V_{rev} as in Fig. 3 B with either Cs$^+$ (Cs_{int}) or NMDG ($NMDG_{int}$) as the major intracellular cation. For comparison, the Q_{ON}-V of Ca$_v$1.3$_L$ in $NMDG_{int}$ is illustrated (*line* taken from Fig. 3 B). (*Inset*) Statistical comparison of the $V_{0.5}$ values (Cs_{int}: -20 ± 1 mV, $n = 9$; $NMDG_{int}$: -29 ± 3 mV, $n = 12$; $p = 0.022$, Student's t-test). (C) Normalized G/G_{max} to normalized $Q_{ON}/Q_{ON,max}$ (replotted from Fig. 3 D as 1-$Q_{ON, post-pre}/Q_{ON, max}$). (D) $V_{0.5}(I_{Ca})$ values for Ca$_v$1.3$_L$, recorded with different internal and external cation-based solutions, as indicated (for solution composition, see Methods) ($n \geq 9$). For calculation of statistical significance, one-way ANOVA with Bonferroni post-hoc test was performed ($p < 0.05$, *; $p < 0.005$, **; $p < 0.001$, ***).

changes in the kinetics and gating of Ca$_v$1.2 currents (24,33), including a shift of the I_{Ca}-V relationship to potentials that are more hyperpolarized (33). However, they do not affect the voltage-dependence of Q_{ON} (24,33).

Here we clearly demonstrate that the more-negative activation range of Ca$_v$1.3 as compared to Ca$_v$1.2 is not due to a more efficient coupling. Instead, coupling is even weaker, as evident from a higher fractional Q_{ON} required for $V_{0.5}(I_{Ca})$. However, Q_{ON} of Ca$_v$1.3 displayed a steeper voltage-dependence and thereby still permits a more-negative I_{Ca}-V. We show that this is in contrast to the mechanism imposed by alternative splicing. We found that in the absence of the CTM, the Q_{ON}-V does not change but more channel activation (i.e., fractional conductance) is observed at a given percentage of maximal Q_{ON}. Similar to the findings obtained with FPL64176 (24), this can be interpreted as more efficient coupling between voltage-sensor movements and pore opening.

It is unclear how the CTM can moderate this coupling. Molecular studies using mutant and chimeric channel constructs will be difficult to perform because this modulatory domain is part of a larger structure consisting not only of the two noncovalently interacting putative α-helices (PCRD, DCRD) of the modulatory domain itself but also of channel-bound CaM (18,34). Based on our observations, it is most likely that the CTM targets the interaction of pore-forming helices (primarily S6) with the S4-S5 linkers that are considered the main structural determinants of Q_{ON}-V to pore opening (22,23,35,36). Another possibility is interference of the distal C-terminus with the channels II-III linker. Such an interaction, which is also modulated by A-kinase anchoring proteins, has recently been described in Ca$_v$1.2 α_1-subunits (37).

What structural differences mediate the steeper voltage-dependence of Ca$_v$1.3 and the higher coupling efficiency of Ca$_v$3.1? The amino-acid sequence within the S4 segments including the positive charges of Ca$_v$1.3 and Ca$_v$1.2 are highly conserved (see alignment in Fig. S1 in the Supporting Material) and are unlikely to explain the difference in their Q_{ON}-V relationships. Structural features outside S4 must therefore play a crucial role. Mutations in S6 segments forming the activation gate or the S5-S6 linker, which couples voltage-sensors to the gate, can induce Q_{ON}-V shifts

to voltages that are more negative. This has been reported by us (for $Ca_v1.3$ (3)) and others (for $Ca_v3.2$ and $Ca_v2.3$ (35,38)). Interdomain cytoplasmic linkers (shown for N-terminal regions of the I-II loop in the case of Ca_v3 channels) can also affect the voltage-dependence of Q_{ON}-V by serving as a 'gating brake' (29). The high sequence similarity of $Ca_v1.3$ α_1 subunits with $Ca_v1.2$ also outside S4 regions provides an excellent opportunity to identify the structural determinants accounting for its uniquely steep voltage-dependence using chimeric approaches.

The high coupling efficiency of $Ca_v3.1$ channels is also not readily explained by charge differences in the S4 segments (see Fig. S1). Assuming that all four voltage sensors have to move completely for pore opening, the fact that only ~25% of Q_{ON} charge are moved when conductance is already fully activated (Fig. 2) could indicate that the activation of only one of the four voltage sensors is sufficient for activating the channel gate.

During the course of our studies, we also discovered that intracellular organic cations sensitize voltage-responses of all three VGCCs investigated. A shift to more negative I_{Ca}-V was initially observed when intracellular Cs^+ was replaced by NMDG, but was also found for Tris and TEA. In contrast to splicing, NMDG affected Q_{ON}-V with no major change in pore coupling, suggesting that it primarily affects voltage sensing itself. This also demonstrates that ion permeation is not required for this voltage shift. This modulation is unlikely to have been caused by a high affinity interaction with NMDG; it was not observed when only 15 mM of Cs^+ were replaced by NMDG ($n = 4$, not shown).

To investigate the possibility of passive charge screening effects, we measured changes in $Ca_v1.3_L$ gating with all possible combinations of equimolar concentrations of NMDG and Cs^+ in the intra- and extracellular solutions. Considerably less is known about passive-charge-screening effects of organic cations as compared to mono- or divalent inorganic cations (39–43). Therefore, although unlikely, the possibility of passive charge screening effects cannot be completely excluded. Alternatively, intracellular organic cations may somehow more specifically interfere with the gating apparatus. An example has previously been described for $K_v1.2$ channels (44) by showing that internal cations are able to occupy the inner cavity of the open channel. Thereby they prevent closing of the inner pore gate and stabilize the open state of the voltage sensors (44). This was not associated with a shift in Q_{ON}-V, but caused a slowing of off-gating currents, especially with such larger cations as NMDG and TEA. However, we were not able to detect a major off-gating current-stabilizing effect of NMDG on $Ca_v1.3_L$ ($n \geq 9$, not shown) or a slowing of I_{Ca} deactivation kinetics.

Independent from the molecular mechanism, our findings clearly emphasize that recording buffer compositions have to be considered when comparing biophysical parameters across different studies examining the voltage-dependent gating properties of VGCCs.

SUPPORTING MATERIAL

REFERENCES

1. Namkung, Y., N. Skrypnyk, …, H. S. Shin. 2001. Requirement for the L-type Ca^{2+} channel $\alpha 1D$ subunit in postnatal pancreatic β-cell generation. *J. Clin. Invest.* 108:1015–1022.

2. Platzer, J., J. Engel, …, J. Striessnig. 2000. Congenital deafness and sinoatrial node dysfunction in mice lacking class D L-type Ca^{2+} channels. *Cell.* 102:89–97.

3. Baig, S. M., A. Koschak, …, H. J. Bolz. 2011. Loss of $Ca_V1.3$ (CACNA1D) function in a human channelopathy with bradycardia and congenital deafness. *Nat. Neurosci.* 14:77–84.

4. Striessnig, J., and A. Koschak. 2008. Exploring the function and pharmacotherapeutic potential of voltage-gated Ca^{2+} channels with gene knockout models. *Channels (Austin).* 2:233–251.

5. Marcantoni, A., V. Carabelli, …, E. Carbone. 2008. Calcium channels in chromaffin cells: focus on L and T types. *Acta Physiol. (Oxf.).* 192:233–246.

6. Mangoni, M. E., B. Couette, …, J. Nargeot. 2003. Functional role of L-type $Ca_v1.3$ Ca^{2+} channels in cardiac pacemaker activity. *Proc. Natl. Acad. Sci. USA.* 100:5543–5548.

7. Marcantoni, A., D. H. Vandael, …, E. Carbone. 2010. Loss of $Ca_v1.3$ channels reveals the critical role of L-type and BK channel coupling in pacemaking mouse adrenal chromaffin cells. *J. Neurosci.* 30:491–504.

8. Striessnig, J., H. J. Bolz, and A. Koschak. 2010. Channelopathies in $Ca_v1.1$, $Ca_v1.3$, and $Ca_v1.4$ voltage-gated L-type Ca^{2+} channels. *Pflugers Arch.* 460:361–374.

9. Koschak, A., D. Reimer, …, J. Striessnig. 2001. Alpha 1D ($Ca_v1.3$) subunits can form l-type Ca^{2+} channels activating at negative voltages. *J. Biol. Chem.* 276:22100–22106.

10. Xu, W., and D. Lipscombe. 2001. Neuronal $Ca_V1.3\alpha_1$ L-type channels activate at relatively hyperpolarized membrane potentials and are incompletely inhibited by dihydropyridines. *J. Neurosci.* 21:5944–5951.

11. Tan, B. Z., F. Jiang, …, T. W. Soong. 2011. Functional characterization of alternative splicing in the C terminus of L-type $Ca_V1.3$ channels. *J. Biol. Chem.* 286:42725–42735.

12. Olson, P. A., T. Tkatch, …, D. J. Surmeier. 2005. G-protein-coupled receptor modulation of striatal $Ca_v1.3$ L-type Ca^{2+} channels is dependent on a Shank-binding domain. *J. Neurosci.* 25:1050–1062.

13. Chan, C. S., J. N. Guzman, …, D. J. Surmeier. 2007. 'Rejuvenation' protects neurons in mouse models of Parkinson's disease. *Nature.* 447:1081–1086.

14. Surmeier, D. J., J. N. Guzman, and J. Sanchez-Padilla. 2010. Calcium, cellular aging, and selective neuronal vulnerability in Parkinson's disease. *Cell Calcium.* 47:175–182.

15. Catterall, W. A., E. Perez-Reyes, …, J. Striessnig. 2005. International Union of Pharmacology. XLVIII. Nomenclature and structure-function relationships of voltage-gated calcium channels. *Pharmacol. Rev.* 57:411–425.

16. Perez-Reyes, E. 2003. Molecular physiology of low-voltage-activated t-type calcium channels. *Physiol. Rev.* 83:117–161.

17. Singh, A., D. Hamedinger, …, J. Striessnig. 2006. C-terminal modulator controls Ca^{2+}-dependent gating of Ca$_v$1.4 L-type Ca^{2+} channels. *Nat. Neurosci.* 9:1108–1116.

18. Singh, A., M. Gebhart, …, A. Koschak. 2008. Modulation of voltage- and Ca^{2+}-dependent gating of Ca$_v$1.3 L-type calcium channels by alternative splicing of a C-terminal regulatory domain. *J. Biol. Chem.* 283:20733–20744.

19. Bock, G., M. Gebhart, …, A. Koschak. 2011. Functional properties of a newly identified C-terminal splice variant of Ca$_v$1.3 L-type Ca^{2+} channels. *J. Biol. Chem.* 286:42736–42748.

20. Striessnig, J., A. Pinggera, G. Kaur, G. Bock, and P. Tuluc. 2014. L-type calcium channels in heart and brain. *WIREs Membr Transp Signal.* 2014. http://dx.doi.org/10.1002/wmts.102.

21. Liu, X., P. S. Yang, …, D. T. Yue. 2010. Enzyme-inhibitor-like tuning of Ca^{2+} channel connectivity with calmodulin. *Nature.* 463:968–972.

22. Jensen, M. O., V. Jogini, …, D. E. Shaw. 2012. Mechanism of voltage gating in potassium channels. *Science.* 336:229–233.

23. Catterall, W. A. 2010. Ion channel voltage sensors: structure, function, and pathophysiology. *Neuron.* 67:915–928.

24. McDonough, S. I., Y. Mori, and B. P. Bean. 2005. FPL 64176 modification of Ca$_v$1.2 L-type calcium channels: dissociation of effects on ionic current and gating current. *Biophys. J.* 88:211–223.

25. Lieb, A., A. Scharinger, …, J. Striessnig. 2012. Structural determinants of Ca$_v$1.3 L-type calcium channel gating. *Channels (Austin).* 6:197–205.

26. Jones, L. P., S. K. Wei, and D. T. Yue. 1998. Mechanism of auxiliary subunit modulation of neuronal α1E calcium channels. *J. Gen. Physiol.* 112:125–143.

27. Perez-Reyes, E., L. L. Cribbs, …, J. H. Lee. 1998. Molecular characterization of a neuronal low-voltage-activated T-type calcium channel. *Nature.* 391:896–900.

28. Perez-Reyes, E., and P. Lory. 2006. Molecular biology of T-type calcium channels. *CNS Neurol. Disord. Drug Targets.* 5:605–609.

29. Karmažínová, M., J. P. Baumgart, …, L. Lacinová. 2011. The voltage dependence of gating currents of the neuronal Ca$_v$3.3 channel is determined by the gating brake in the I-II loop. *Pflugers Arch.* 461:461–468.

30. Long, S. B., X. Tao, …, R. MacKinnon. 2007. Atomic structure of a voltage-dependent K$^+$ channel in a lipid membrane-like environment. *Nature.* 450:376–382.

31. Payandeh, J., T. Scheuer, …, W. A. Catterall. 2011. The crystal structure of a voltage-gated sodium channel. *Nature.* 475:353–358.

32. Perez-Reyes, E. 2010. Characterization of the gating brake in the I-II loop of Ca$_v$3 T-type calcium channels. *Channels (Austin).* 4:453–458.

33. Fan, J. S., Y. Yuan, and P. Palade. 2000. Kinetic effects of FPL 64176 on L-type Ca^{2+} channels in cardiac myocytes. *Naunyn Schmiedebergs Arch. Pharmacol.* 361:465–476.

34. Johny, M. B., P. S. Yang, …, D. T. Yue. 2013. Dynamic switching of calmodulin interactions underlies Ca^{2+} regulation of Cav1.3 channels. *Nat. Com.* 4:1717.

35. Wall-Lacelle, S., M. I. Hossain, …, L. Parent. 2011. Double mutant cycle analysis identified a critical leucine residue in the IIS4S5 linker for the activation of the Ca$_v$2.3 calcium channel. *J. Biol. Chem.* 286:27197–27205.

36. Haddad, G. A., and R. Blunck. 2011. Mode shift of the voltage sensors in *Shaker* K$^+$ channels is caused by energetic coupling to the pore domain. *J. Gen. Physiol.* 137:455–472.

37. Altier, C., S. J. Dubel, …, E. Bourinet. 2012. AKAP79 modulation of L-type channels involves disruption of intramolecular interactions in the Ca$_v$1.2 subunit. *Channels (Austin).* 6:157–165.

38. Demers-Giroux, P. O., B. Bourdin, …, L. Parent. 2013. Cooperative activation of the T-type Ca$_v$3.2 channel: interaction between domains II and III. *J. Biol. Chem.* 288:29281–29293.

39. Abdulkader, F., M. Arcisio-Miranda, …, J. Procopio. 2007. Surface potential determination in planar lipid bilayers: a simplification of the conductance-ratio method. *J. Biochem. Biophys. Methods.* 70:515–518.

40. McLaughlin, S. G., G. Szabo, and G. Eisenman. 1971. Divalent ions and the surface potential of charged phospholipid membranes. *J. Gen. Physiol.* 58:667–687.

41. Green, W. N., and O. S. Andersen. 1991. Surface charges and ion channel function. *Annu. Rev. Physiol.* 53:341–359.

42. Wilson, D. L., K. Morimoto, …, A. M. Brown. 1983. Interaction between calcium ions and surface charge as it relates to calcium currents. *J. Membr. Biol.* 72:117–130.

43. Becchetti, A., A. Arcangeli, …, E. Wanke. 1992. Intra- and extracellular surface charges near Ca^{2+} channels in neurons and neuroblastoma cells. *Biophys. J.* 63:954–965.

44. Goodchild, S. J., H. Xu, …, D. Fedida. 2012. Basis for allosteric open-state stabilization of voltage-gated potassium channels by intracellular cations. *J. Gen. Physiol.* 140:495–511.